nature genetics

LETTERS

https://doi.org/10.1038/s41588-018-0251-4

Germline *HAVCR2* mutations altering TIM-3 characterize subcutaneous panniculitis-like T cell lymphomas with hemophagocytic lymphohistiocytic syndrome

Tenzin Gayden[1,32], Fernando E. Sepulveda[2,32], Dong-Anh Khuong-Quang[3,4,32], Jonathan Pratt[1,32], Elvis T. Valera[1,5], Alexandrine Garrigue[2], Susan Kelso[6,7], Frank Sicheri[6,7], Leonie G. Mikael[1], Nancy Hamel[8], Andrea Bajic[1], Rola Dali[9], Shriya Deshmukh[10], Dzana Dervovic[6], Daniel Schramek[6,7], Frédéric Guerin[2], Mikko Taipale[7], Hamid Nikbakht[1,9], Jacek Majewski[1,11], Despina Moshous[12], Janie Charlebois[13], Sharon Abish[13], Christine Bole-Feysot[14], Patrick Nitschke[15], Brigitte Bader-Meunier[12], David Mitchell[13], Catherine Thieblemont[16,17], Maxime Battistella[17,18], Simon Gravel[11], Van-Hung Nguyen[19], Rachel Conyers[3,4], Jean-Sebastien Diana[12], Chris McCormack[20,21], H. Miles Prince[22,23], Marianne Besnard[24], Stephane Blanche[12], Paul G. Ekert[3,4], Sylvie Fraitag[25], William D. Foulkes[1,8], Alain Fischer[12,26,27], Bénédicte Neven[12,27,33], David Michonneau[17,28,33], Geneviève de Saint Basile[2,29,33*] and Nada Jabado[1,30,31,33*]

Subcutaneous panniculitis-like T cell lymphoma (SPTCL), a non-Hodgkin lymphoma, can be associated with hemophagocytic lymphohistiocytosis (HLH), a life-threatening immune activation that adversely affects survival[1,2]. T cell immunoglobulin mucin 3 (TIM-3) is a modulator of immune responses expressed on subgroups of T and innate immune cells. We identify in ~60% of SPTCL cases germline, loss-of-function, missense variants altering highly conserved residues of TIM-3, c.245A>G (p.Tyr82Cys) and c.291A>G (p.Ile97Met), each with specific geographic distribution. The variant encoding p.Tyr82Cys TIM-3 occurs on a potential founder chromosome in patients with East Asian and Polynesian ancestry, while p.Ile97Met TIM-3 occurs in patients with European ancestry. Both variants induce protein misfolding and abrogate TIM-3's plasma membrane expression, leading to persistent immune activation and increased production of inflammatory cytokines, including tumor necrosis factor-α and interleukin-1β, promoting HLH and SPTCL. Our findings highlight HLH-SPTCL as a new genetic entity and identify mutations causing TIM-3 alterations as a causative genetic defect in SPTCL. While HLH-SPTCL patients with mutant TIM-3 benefit from immunomodulation, therapeutic repression of the TIM-3 checkpoint may have adverse consequences.

[1]Department of Human Genetics, McGill University, Montreal, Quebec, Canada. [2]Laboratory of Normal and Pathological Homeostasis of the Immune System, INSERM U1163, Institut Imagine, and Université Paris Descartes-Sorbonne Paris Cité, Paris, France. [3]Children's Cancer Center, The Royal Children's Hospital and Murdoch Children's Research Institute, Parkville, Victoria, Australia. [4]Department of Pediatrics, University of Melbourne, Parkville, Victoria, Australia. [5]Department of Pediatrics, Ribeirão Preto Medical School, University of São Paulo, São Paulo, Brazil. [6]Lunenfeld-Tanenbaum Research Institute, Sinai Health System, Toronto, Ontario, Canada. [7]Department of Molecular Genetics, University of Toronto, Toronto, Ontario, Canada. [8]Cancer Research Program, Research Institute of the McGill University Health Center, Montreal, Quebec, Canada. [9]Canadian Centre for Computational Genomics, Montreal, Quebec, Canada. [10]Department of Experimental Medicine, McGill University, Montreal, Quebec, Canada. [11]McGill University and Genome Quebec Innovation Center, Montreal, Quebec, Canada. [12]Department of Pediatric Immunology and Hematology, Hôpital Necker-Enfants Malades, Assistance Publique-Hôpitaux de Paris (AP-HP), Paris, France. [13]Division of Hematology and Oncology, Montreal Children's Hospital, McGill University Health Centre, Montreal, Quebec, Canada. [14]Plateforme de Génomique, Institut Imagine, Paris, France. [15]Plateforme de Bioinformatique, Université Paris Descartes, Université Sorbonne Paris Cité, Paris, France. [16]Hematology and Oncology Unit, Saint Louis Hospital, Paris, France. [17]Paris Diderot University, Université Sorbonne Paris Cité, Paris, France. [18]Cytology and Pathology Laboratory, Saint Louis Hospital, Paris, France. [19]Department of Pathology, Montreal Children's Hospital, McGill University Health Centre, Montreal, Quebec, Canada. [20]Department of Surgical Oncology, Peter MacCallum Cancer Institute, University of Melbourne, Melbourne, Victoria, Australia. [21]Department of Dermatology, St. Vincent's Hospital, Fitzroy, Victoria, Australia. [22]Epworth Healthcare, Melbourne, Victoria, Australia. [23]Department of Medical Oncology, Sir Peter MacCallum Cancer Centre and University of Melbourne, Melbourne, Victoria, Australia. [24]Department of Neonatology, Centre Hospitalier de Polynésie Française, Papeete, French Polynesia. [25]Department of Anatomy and Cytology/Pathology, Centre Hospitalier Universitaire Paris, Hôpital Necker-Enfants Malades, Paris, France. [26]Collège de France, Paris, France. [27]INSERM U1163, Institut Imagine and Université Paris Descartes -Sorbonne Paris Cité, Paris, France. [28]Hematology and Transplantation Unit, Saint Louis Hospital, Paris, France. [29]Centre d'Etudes des Déficits Immunitaires, Centre Hospitalier Universitaire Paris, Hôpital Necker-Enfants Malades, Paris, France. [30]Department of Pediatrics, McGill University, Montreal, Quebec, Canada. [31]Research Institute, McGill University Health Centre, Montreal, Quebec, Canada. [32]These authors contributed equally: Tenzin Gayden, Fernando E. Sepulveda, Dong-Anh Khuong-Quang, Jonathan Pratt.[33]These authors jointly supervised this work: Bénédicte Neven, David Michonneau, Geneviève de Saint Basile, Nada Jabado. *e-mail: genevieve.de-saint-basile@inserm.fr; nada.jabado@mcgill.ca

Table 1 | Clinical, demographic and histological features of TIM-3 mutant SPTCL patients analyzed in this study

Patient	*HAVCR2* (TIM-3)	Germline status	Ethnicity	Gender	Age at onset	Signs of HLH[a]	Panniculitis	TCR rearrangement in skin	Adipocyte rimming in BM	Outcome
P1	Y82C	Homozygous	East Asian	Male	11	+; R	U, L, T	Monoclonal	Yes	CR post-allogeneic HSCT
P2	Y82C	Homozygous	East Asian	Female	9	+	L, buttocks	Monoclonal	Yes	CR post-allogeneic HSCT
P3	Y82C	Homozygous	Polynesian	Female	13	+/−	U, L, T	Oligoclonal	NA	CR
P4	Y82C	Homozygous	Polynesian	Male	11	+; R	U, L, T	Monoclonal	NA	SD, maintenance therapy
P5	Y82C	Homozygous	Polynesian	Female	12	+	L, T, buttocks, face	Monoclonal	Yes	CR post-autologous HSCT
P6	Y82C	Homozygous	Polynesian	Male	1	+/−	L, T, face	NA	Yes	CR
P7	Y82C[b]	NA	Polynesian	Female	16	+/−; R	U, L, T	Monoclonal	Yes	SD, maintenance therapy
P8	Y82C[b]	NA	East Asian	Male	67	+/−; R	U, L, T	Polyclonal	Yes	CR, maintenance therapy
P9	Y82C[b]	NA	Polynesian	Female	22	+	U, L, T	Monoclonal	Yes	CR, autologous HSCT and immunosuppression
P10	Y82C	Homozygous	East Asian	Female	41	+/−	U, L, T	Monoclonal	Yes	CR post-allogeneic HSCT
P11	Y82C	Homozygous	East Asian	Male	48	+	T	Monoclonal	NA	Recent diagnosis
P12	Y82C	Homozygous	Polynesian	Male	31	+/−	L	NA	Yes	SD, maintenance therapy
P13	I97M[b]	NA	Caucasian	Female	90	−	U, L	Monoclonal	NA	CR
P14	I97M	Homozygous	Caucasian	Female	15	−	L	Monoclonal	Yes	CR, maintenance therapy
P15	I97M[c]	Heterozygous	Caucasian	Male	11	+; R	U, L, T	Monoclonal	Yes	CR, maintenance therapy
P16	Y82C[c] and I97M[c]	NA	North African	Female	31	+/−	U, L, T	Monoclonal	No	CR

BM, bone marrow; CR, complete remission; L, lower limb; NA, not available; SD, stable disease; T, trunk; U, upper limb. [a]+, complete criteria of HLH met; +/−, incomplete criteria of HLH met; R, relapse. [b]Homozygous in the tumor. [c]Heterozygous in the tumor.

Subcutaneous panniculitis-like T cell lymphoma (SPTCL) is an uncommon cytotoxic T cell non-Hodgkin lymphoma[3] in which $CD8^+$ T cells that express α/β T cell antigen receptors (TCRs) infiltrate subcutaneous adipose tissue, rimming adipocytes in a lace-like pattern[1,2]. Both children[4] and adults can be affected, with a median age at diagnosis of 36 years and a female gender bias[1,5]. Affected individuals typically present with multiple subcutaneous nodules, systemic B-cell symptoms, and, in ~20% of cases, associated autoimmune disorders, most commonly systemic lupus erythematosus[5,6]. SPTCL can follow a fulminant course when associated with hemophagocytic lymphohistiocytosis (HLH)[3], which accompanies ~20% of cases[5] and decreases 5 year survival from 90% to less than 50%[1,7]. There is no standardized therapy, and although multidrug chemotherapy and radiotherapy are commonly used, immunosuppressive regimens, particularly cyclosporine A, seem more effective, possibly owing to the immunologic features of this lymphoma[8,9]. The underlying genetic cause of SPTCL remains unknown, but a familial predisposition has been suggested[9], and in one case, disease transmission following allogeneic hematopoietic stem cell transplant (HSCT)[10] was reported.

Here we studied a series of 27 SPTCLs to identify genetic variants underlying this disease. All samples were collected with informed consent following approval of the institutional review boards of the respective institutions. We performed whole-exome sequencing (WES) on 17 cases and further validated results by targeted sequencing on all cases included in this series (Table 1 and Supplementary Tables 1–3). We identified missense variants in *HAVCR2*, which encodes T cell immunoglobulin mucin 3 (TIM-3), with c.245A>G (p.Tyr82Cys; NP_116171) and c.291A>G (p.Ile97Met; NP_116171) observed in 16 of 27 patients (Table 1 and Supplementary Note). Upon examination of patients' ethnic origins, the 12 SPTCL patients of Polynesian and East Asian origin harbored the homozygous p.Tyr82Cys TIM-3 missense variant in tumors and in the corresponding germline in 10 of 16 patients for whom this material was available (Table 1). This included the two affected East Asian sibling pairs P1/P2 and P10/P11 from two distinct families. In these and the two Polynesian families with material available, parents were heterozygous carriers while unaffected siblings were wild-type or heterozygous carriers, except for a healthy brother of P4, currently aged 20, who was homozygous for p.Tyr82Cys TIM-3 and showed increased immunoglobulin E (IgE) levels and positive anti-DNA antibodies when investigated (Fig. 1a, Table 1, and Supplementary Table 1). In three patients of European ancestry, we identified the germline variant encoding p.Ile97Met in TIM-3, which was homozygous in two (P12 and P13) and heterozygous in one (P15) in the germline but with no TIM-3 plasma membrane expression in the tumor (Fig. 1b–d, Table 1, and Supplementary Table 1). P16, of North African origin, was compound heterozygous for p.[Tyr82Cys]+[Ile97Met] TIM-3 in tumor material (Table 1). However, based on lack of additional material, we could not identify the haplotype phase or germline status of these variants. There were no other relevant or recurrent mutations on analyses of the WES dataset, including for the 11 SPTCLs wild-type for TIM-3, which were from patients of European (10) or South American (1) descent (Supplementary Table 3). TIM-3 is a member of the TIM family and is expressed by several cell types of the immune system[11]. Through interactions with cognate ligands, the best characterized being galectin-9, TIM-3 acts as a negative immune checkpoint regulating peripheral tolerance, antitumoral immunity, and innate immune responses[12,13]. p.Tyr82Cys and p.Ile97Met TIM-3 are predicted to be deleterious in silico by PolyPhen-2 (PolyPhen-2 = 1) and CADD scores (>15), although SIFT considered them as benign (>0.75). These variants are highly conserved across species (phastCons > 350), as well as among other TIM family members (Fig. 1b).

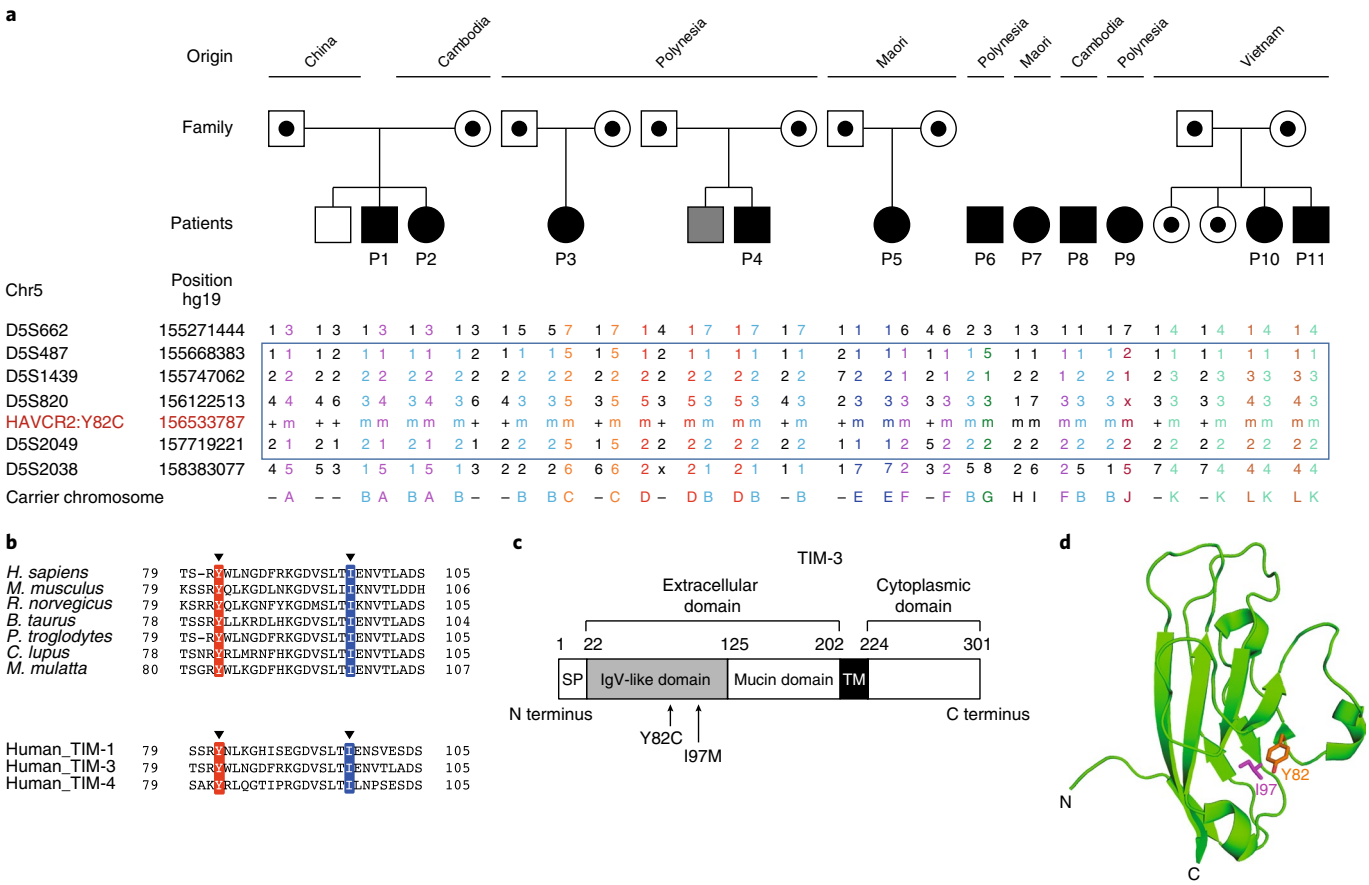

Fig. 1 | Haplotype segregation in the Tyr82Cys (Y82C)-patient families and localization of the two altered residues on the TIM-3 protein. a, Pedigrees showing 11 patients with Y82C TIM-3 (*HAVCR2*) and their relatives available for genotyping and/or sequencing. Circles denote female family members, squares denote male family members, black symbols denote affected family members with homozygous Y82C TIM-3 variant (m m), the gray symbol denotes the healthy family member with homozygous Y82C variant who had anti-DNA antibodies and increased IgE levels (m m), and open symbols denote unaffected family members with no (+ +) or heterozygous (+ m) (black dot) Y82C TIM-3 variant. Haplotype reconstruction from genotyping data using six microsatellite markers flanking *HAVCR2* is shown. Haplotypes are drawn with several colors to distinguish segregation in families. A region of consecutive conserved alleles in several individuals (light blue haplotype) suggests a founder effect. Chromosomes bearing the Y82C variant where haplotype phase was conclusively determined via segregation in the family are in bold, while haplotypes where phase is not definitively known are not. **b**, Sequence alignments showing homology between the IgV-like domain of the TIM-3 protein from different species (*Homo sapiens*, *Mus musculus*, *Rattus norvegicus*, *Bos taurus*, *Pan troglodytes*, *Canis lupus*, and *Macaca mulatta*) as well as between the human TIM family members, highlighting the strong conservation of the two variant residues Y82C (in red) and Ile97Met (I97M) (in blue). **c**, Schematic representation of the human TIM-3 protein with the localization of the two variant residues. The regions corresponding to the signal peptide sequence (SP), the immunoglobulin-like domain (IgV-like domain), and the transmembrane domain (TM) are shown. **d**, Structure of the human TIM-3 IgV domain highlighting the sites of the misfolding substitutions at Tyr82 (Y82) and Ile97 (I97) (Protein Data Bank ID: 5F71).

They map to the membrane distal immunoglobulin variable (IgV) domain of the protein (Fig. 1c,d), which is critical for engaging galectin-9 and TIM-3 function in terminating immune responses[14]. p.Tyr82Cys and p.Ile97Met in TIM-3 have been documented in dbSNP (rs184868814 and rs35960726), with global minor allele frequency (MAFs) of 0.0036 and 0.002908, respectively, in the Exome Aggregation Consortium (ExAC) or Genome Aggregation Database (gnomAD). p.Tyr82Cys is more prevalent in East Asians (MAF = 0.02104) and rare in Europeans (Supplementary Fig. 2). Consistent with the expected allele frequency, four individuals were homozygous for p.Tyr82Cys in ExAC (three East Asian, one Latino), but lack of informed consent prevented us from identifying and contacting them. This indicates an incomplete penetrance and/or the presence of misdiagnosed cases, the former supported by the delay in disease onset for some patients and the apparently asymptomatic healthy brother of P4. Whether genetic and/or environmental modifiers influence disease penetrance warrants further investigation. p.Ile97Met is more frequent in Caucasians (Finnish MAF = 0.002365, non-Finnish MAF = 0.004942) and is not reported in Asian populations. As the Polynesian population is understudied, we acquired germline DNA from 107 healthy individuals from Tahiti (Polynesia) and identified heterozygosity for p.Tyr82Cys TIM-3 in eight individuals, which leads to an estimated allele frequency of 4×10^{-2}. Thus, the expected frequency of homozygotes should be 16×10^{-4}, a number that would roughly double based on the estimated 4% rate of inbreeding in Polynesia[15]. Given that there are seven Polynesian patients carrying the p.Tyr82Cys homozygous variant in our series, we estimated the probability that this could have occurred by chance to be less than 2.7×10^{-18}. The transmission pattern in kindreds, the pathogenesis of the disease, and the known role of TIM-3 in modulating immune functions[16,17], with absence of other shared variants in germline and SPTCL samples, support p.Tyr82Cys and p.Ile97Met TIM-3 as the most valid candidate variants contributing to disease in these SPCTL patients.

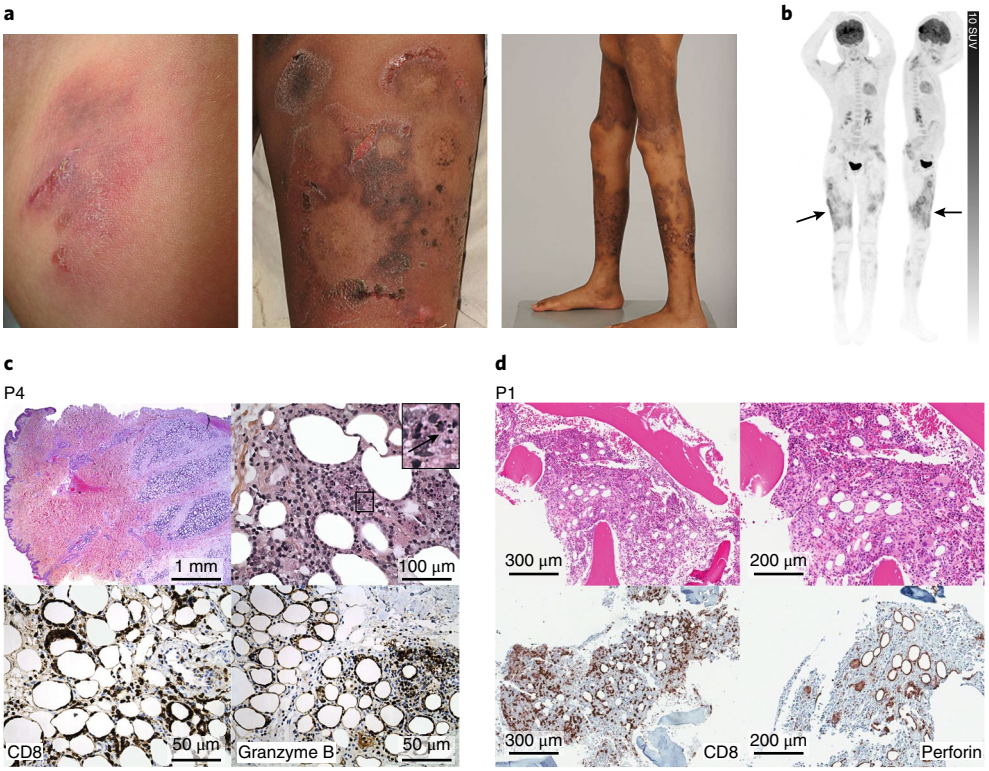

Fig. 2 | Clinical and histological features of subjects with TIM-3 deficiency. a, Photographs showing the cutaneous manifestations in two patients, with localized bluish subcutaneous nodules in the inguinal region in P14 and multiple erythematous ulcerated plaques and subcutaneous nodules on the lower extremities in P5. **b**, PET scan analysis showing hyperactive lesions in subcutaneous tissues of P5 (arrows). SUV, standardized uptake value. **c**, Histologic section of a subcutaneous nodule from P4 showing dense cellular infiltrates involving the subcutaneous fat (hematoxylin and eosin staining) while the dermis is preserved. Atypical lymphoid cells rimming adipocytes and signs of hemophagocytosis (arrow in the inset) can be observed. The lymphocytes expressed CD3, CD8, and granzyme B. **d**, Histologic section showing the unusual adipocyte rimming in the bone marrow of P1 by an immune cell, mirroring what is seen in the skin. Fig. 2c and 2d illustrate adipocyte rimming by immune cells enriched for cytotoxic lymphocytes ($CD8^+$/$perforin^+$/$granzyme^+$) in sub-cutaneous tissue (panniculitis) and in the bone marrow.

Since the p.Tyr82Cys variant appears enriched in Polynesian and East Asian populations, we investigated whether these shared a common ancestry in the three kindreds available. Using haplotype analysis and polymorphic short tandem repeat markers spanning the region including *HAVCR2* (TIM-3), we identified at least 12 distinct chromosomal backgrounds carrying the p.Tyr82Cys variant, indicating that p.Tyr82Cys is a recurrent variant in these populations. We also observed the presence of consecutive conserved alleles in several individuals at four short tandem repeat markers flanking the gene. This suggests the presence of a founder chromosome with elevated frequency among these populations, as this ancestral chromosome was present in three families, and potentially in three of four additional unrelated patients who showed consistent genotypes (Fig. 1a). This is consistent with recent findings indicating that Polynesians are of East Asian ancestry[18].

The 16 patients (P1–P16) with TIM-3 alterations (Table 1, Supplementary Table 1, and Supplementary Note) had typical clinical, radiological, and pathological findings of SPTCL (Fig. 2a–c). However, compared with TIM-3 wild-type patients (P17–P27), they showed a much younger median age at onset (15 versus 41 years), with onset below the age of 22 in 10 cases, a longer median time to diagnosis post-onset of clinical symptoms (10 versus 3 months), and a more severe disease course. Also, most TIM-3-mutant SPTCL patients had HLH (14 of 16 versus 3 of 11; $P < 0.01$) and adipocyte rimming on bone marrow biopsies (11 of 13 versus 0 of 11; $P < 0.0001$) (Fig. 2d, Table 1, and Supplementary Table 1). Intensive investigations, including for Epstein-Barr virus, did not identify associated pathogens or a plausible trigger, and the diagnosis of primary cutaneous γδ lymphoma, which is usually accompanied with HLH, was excluded based on the TCR αβ rearrangements identified in tumors (Table 1). The occurrence in younger patients and the severe and refractory course of the disease with improved responses to immunosuppressive regimens, as also observed by others[8], are in keeping with inherited forms of HLH and an underlying immune defect.

In all samples with p.Tyr82Cys and p.Ile97Met mutations, mutant TIM-3 showed an aggregate staining pattern in the peri-Golgi apparatus with limited plasma membrane expression in panniculitis biopsies compared with the expected plasma membrane expression seen in all TIM-3 wild-type samples (Fig. 3a). This was further confirmed by testing peripheral blood mononuclear cells available from P3, P4, and P11, where p.Tyr82Cys TIM-3 mutant expression was absent on peripheral monocytes ($CD14^+$) and, following cell activation, on $CD4^+$ and $CD8^+$ T lymphocytes (Fig. 3b and data not shown). In p.Tyr82Cys TIM-3 heterozygous individuals, membrane expression of the receptor was at an intermediate level (Supplementary Fig. 3a and data not shown). We further validated mistargeted protein expression of mutant TIM-3 in HEK293 cells that were stably transduced to express doxycycline-inducible flag-tagged wild-type, p.Tyr82Cys, or p.Ile97Met TIM-3 (Fig. 3c and Supplementary Fig. 3b). Immunofluorescence and flow cytometry confirmed a drastic decrease of TIM-3 levels at the plasma membrane, as only wild-type TIM-3-transduced cells had detectable TIM-3 surface expression (Fig. 3d and Supplementary

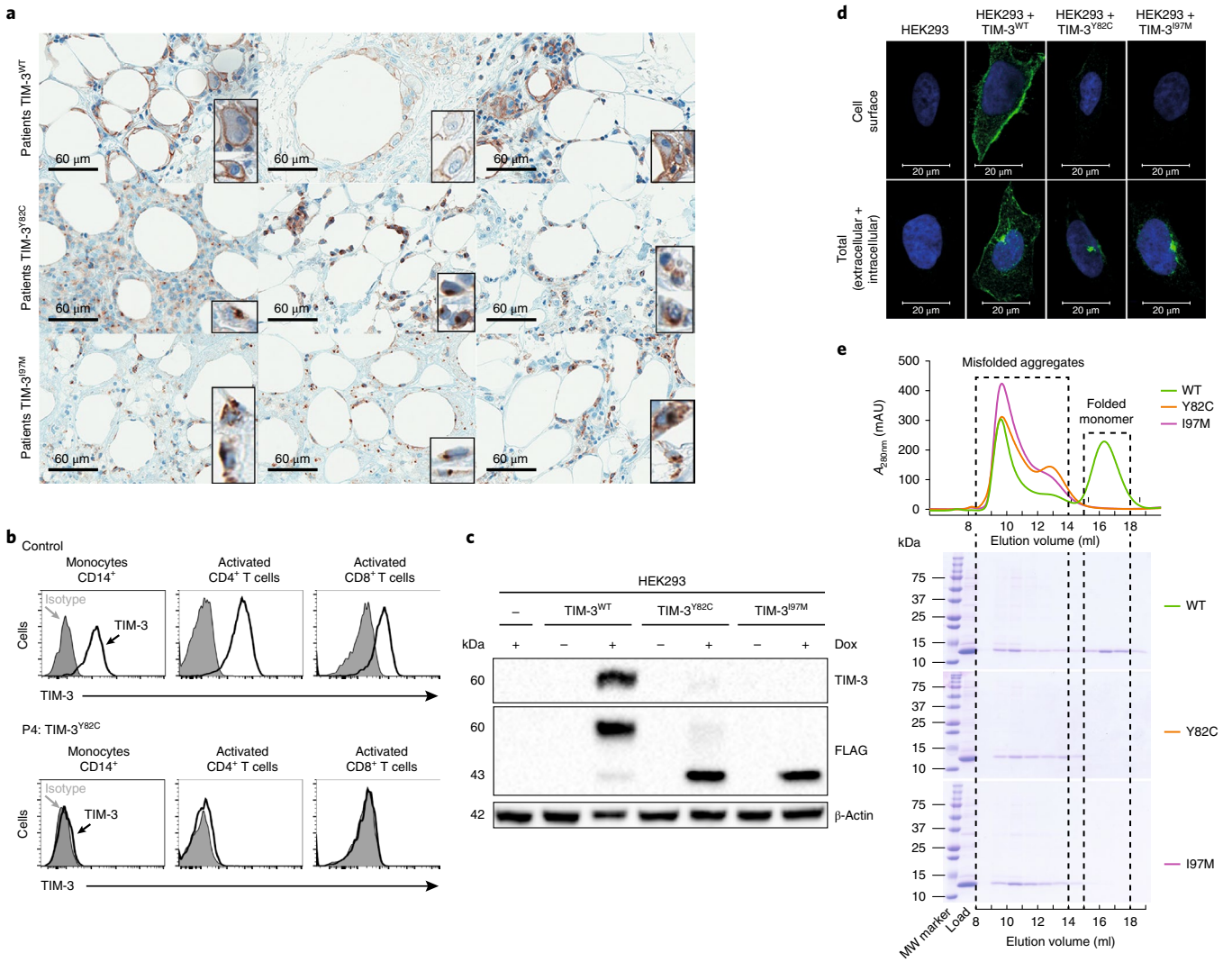

Fig. 3 | Effect of Y82C and I97M variants on TIM-3 expression. a, TIM-3 expression detected by immunohistochemical analysis using anti-TIM-3. TIM-3 is expressed at the cell surface of immune cells in control wild-type (WT) SPTCL (TIM-3^{WT}: P17, P18, and P19, upper panels, left to right), in particular on lymphocytes rimming the adipocytes. In contrast, both TIM-3 mutant proteins display intracellular localization with limited membrane expression in patients' skin samples (TIM-3^{Y82C}: P1, P2, and P7, middle panels, left to right; TIM-3^{I97M}: P13, P14, and P15, lower panels, left to right). Enlarged pictures of individual cells are provided for each panel. Note absence of TIM-3 membrane expression in SPTCL from P15 (lower right panel). **b**, Flow cytometry expression of TIM-3 on monocytes (CD14$^+$) and on CD4$^+$ and CD8$^+$ phytohemagglutinin-induced T lymphoblasts shows TIM-3 plasma membrane expression in control cells but absence of TIM-3 membrane expression on P4's cells. **c**, Immunoblot analysis of TIM-3 expression in whole-cell extracts of HEK293T cells untransduced (control) or transduced with WT TIM-3, Y82C TIM-3, or I97M TIM-3 FLAG-tagged inducible constructs. TIM-3 expression was induced in the presence of doxycycline (Dox) as described in the Online Methods. A transfection efficiency control (anti-FLAG) and a protein-loading control (anti-actin) were used. Expression of the Y82C and I97M TIM-3 mutants was severely impaired, compared with WT TIM-3. Following induction, an immunoblot using an N-terminal IgV domain TIM-3 antibody detected the expected ~62 kDa band only in WT TIM-3 cells, while anti-FLAG (C-terminus) immunoblot detected a smaller 45 kDa band in TIM-3 mutant transfectants. **d**, Confocal microscopy analysis was performed on the same HEK293T cells as in **c**, immunolabeled with anti-TIM-3 (in green) and nuclei counterstained with DAPI (in blue), showing impaired surface expression of the two TIM-3 mutant proteins compared with WT TIM-3. In permeabilized cells, in both Y92C and I97M TIM-3 infected cells, the mutant proteins were present as intracellular aggregates. Experiments in **c** and **d** were repeated three times, and representative images are shown. **e**, Size-exclusion elution profiles and SDS-PAGE analysis of in vitro-refolded WT and the indicated mutants of the TIM-3 IgV domain on a Superdex G-75 column loaded with cell lysates from WT and Y82C or I97M TIM-3-transfected HEK293 cells. Misfolded aggregates are highlighted with arrows. The refolding assay was repeated twice with similar results. mAU, milli-absorbance units; MW, molecular weight.

Fig. 4a). The intracellular peri-Golgi aggregates and lack of TIM-3 detection using the N-terminal TIM-3 antibody suggested protein misfolding, as also predicted by FoldX force-field calculations[19]. This was further confirmed by in vitro protein-folding experiments followed by size-exclusion chromatography (Fig. 3e); by native polyacrylamide gel electrophoresis (PAGE), which showed that only wild-type IgV TIM-3 retained a normal secondary structure migrating at 62 kDa (Supplementary Fig. 4b); and by the disruption of the known amount of IgV domain N-glycosylation[14] (Supplementary Fig. 4c). Taken together, our results show that the Tyr82 and Ile97 are critical residues needed for TIM-3 localization at the cell surface, and that the two identified substitutions impair proper folding and post-translational modifications of the TIM-3 protein.

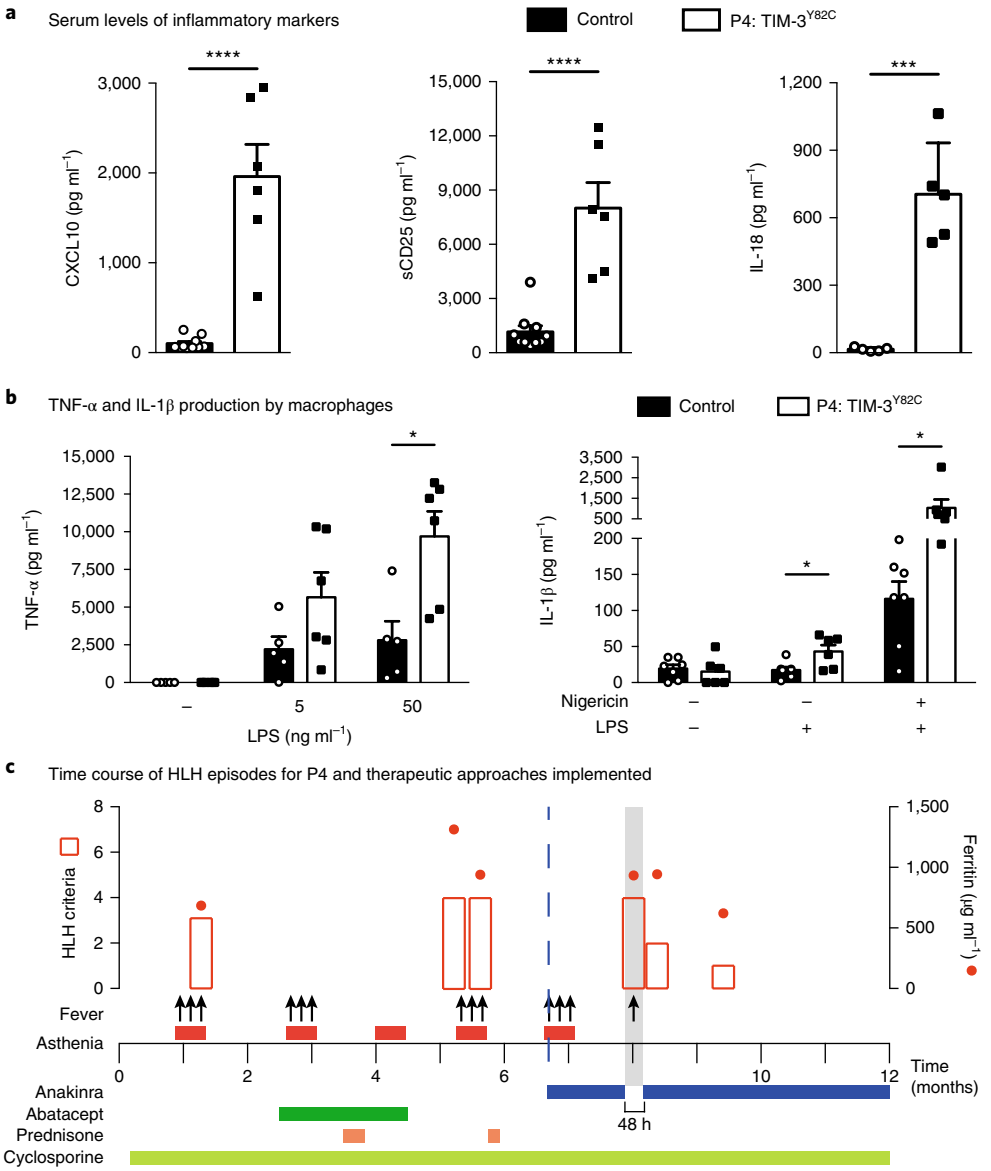

Fig. 4 | Functional effects of the TIM-3 deficiency and IL-1 receptor antagonist treatment in P4. a, Plots showing the high serum levels in P4 (white bars) of inflammatory markers (CXCL10 chemokine, IL-18 cytokine and soluble CD25) compared with controls (black bars); IL-18, sCD25 and CXCL10 were quantified by ELISA (***$P < 0.001$). Statistics were derived from independent biological samples. Data are shown as mean ± s.e.m. (CXCL10: control ($n = 10$) and Y82C ($n = 6$); sCD25: control ($n = 10$) and Y82C ($n = 6$); IL18: control ($n = 5$) and Y82C ($n = 5$). **b**, Plots showing increased TNF-α (left panel) and IL-1β (right panel) production by macrophages from P4 with Y82C TIM-3 mutation compared with WT TIM-3 controls, in response to TLR4 (LPS) and NLRP3 (nigericin) activation. Macrophages were differentiated from $CD14^+$ peripheral monocytes in vitro by culture with recombinant human M-CSF for 5 days. On day 6, macrophages were primed with LPS and stimulated or not with nigericin (NLRP3 agonist). Secretion of TNF-α (left panel) and IL-1β was measured on the supernatant by CBA. Graphs represent mean ± s.e.m. of 6–7 independent experiments (*$P < 0.05$). Statistics were derived from independent biological samples (different cell cultures) (TNF-α: control ($n = 5$) and Y82C ($n = 6$); IL-1β: control ($n = 7$) and Y82C ($n = 6$). **c**, Plots showing the time course of HLH episodes affecting P4 during the past 11 months and the different therapeutic strategies implemented. Depicted are the different episodes of persistent fever (black arrows), the number of positive HLH criteria among six (red bars, left *y* axis), and serum ferritin levels (red dots, right *y* axis). Abatacept was administrated at 1,000 mg every 15 days, prednisone at 0.5 mg per kg every day, and anakinra at 100 mg per day.

HLH appears as a defining feature of TIM-3-mutant SPTCL. Inherited causes of HLH mainly result from impaired granule-dependent cytotoxicity of lymphocytes[20] and were ruled out in our cohort (Supplementary Fig. 5 and data not shown). The TIM-3 negative checkpoint is also a critical regulator of innate immunity and inflammatory responses[12,13]. It suppresses effector T cell (the T_H1 subset of helper T cells) responses by decreasing interferon-γ (IFN-γ)-driven inflammation[12], and defects in its function may thus account for the HLH manifestations seen in TIM-3-mutant SPTCL. Accordingly, in the patient with available material at the time of active disease (P4), we observed elevated serum levels of IFN-γ-induced CXCL10, inflammasome-activated interleukin-18 (IL-18), and soluble CD25, a biochemical signature characteristic of inherited HLH[21] (Fig. 4a and Supplementary Fig. 6). T lymphoblasts from patients were also shown to produce significantly increased amounts of tumor-necrosis factor-α (TNF-α) and IL-2 in vitro (Supplementary Fig. 6a). TIM-3 also regulates monocyte/macrophage activation. In mice, its overexpression correlates with

decreased secretion of inflammatory cytokines upon toll-like receptor (TLR) and inflammasome activation, while its silencing increases NLRP3 (nucleotide-binding leucine-rich pyrin contatining domain 3) inflammasome activity and the production of inflammatory cytokines by macrophages[22]. We therefore assessed these responses by stimulating control or p.Tyr82Cys TIM-3 macrophages with the TLR4 agonist lipopolysaccharide (LPS) followed by treatment with an NLRP3 inflammasome agonist, two stimulation steps required for IL-1β maturation before release[23]. In contrast to control macrophages, monocyte-derived macrophages from p.Tyr82Cys TIM-3 patients secreted more TNF-α in response to LPS stimulation than control cells did (Fig. 4b and Supplementary Fig. 6b). Furthermore, LPS stimulation alone induced significant release of mature IL-1β by TIM-3-mutant P4 macrophages, the level of which was further increased by sequential stimulation with the NLRP3 agonist nigericin (Fig. 4b), while both stimuli were required for IL-1β secretion in TIM-3 wild-type macrophages (Fig. 4b). Increased IL-1β secretion by P3's and P11's macrophages was also seen upon LPS and nigericin stimulation (Supplementary Fig. 6c). These results indicate that misfolding of TIM-3 promotes secretion of inflammatory cytokines and activation of the NLRP3 inflammasome. It is likely that defective TIM-3 function on macrophages lowers the threshold for inflammasome activation, which is dramatically exacerbated upon NLRP3 stimulation in response to a putative trigger. On the basis of these findings, following ethical approval, we treated P4 with anakinra, an IL-1 inhibitor, and obtained symptom resolution and sustained improvement in overall state (Fig. 4c).

An intriguing and central clinical feature of SPTCL is the selective infiltration of pathogenic T cells within the subcutis with no indications of a local infectious trigger. There is a high frequency of regulatory T lymphocytes (T_{reg} cells) within adipose tissues in normal skin[23]. Interestingly, Tim-3$^+$ T_{reg} cells exert a more potent suppressor function than Tim-3$^-$ T_{reg} cells[24], and their depletion in mice results in severe cutaneous inflammation[24]. In keeping with these observations, we identified a drastic decrease in FOXP3$^+$CD4$^+$ T cells in TIM-3 mutants compared with TIM-3 wild-type SPTCL (Supplementary Fig. 7). This further supports the notion that TIM-3 potentially plays a gatekeeper role for inflammation in these tissues. TIM-3 expression is associated with T cell exhaustion in human immunodeficiency virus, multiple sclerosis, and cancer, and therapeutic blockade of this immune checkpoint is increasingly being used to help overcome this phenomenon. This is especially true in cancer, where upregulation of TIM-3 following manipulation of the programmed cell death protein-1 checkpoint limits therapeutic responses and is actively being targeted[25]. Our observation of clinical consequences of TIM-3 deficiency calls for cautious use of this strategy.

In summary, we report a new inherited autosomal recessive condition characterized by HLH–SPTCL that results from TIM-3 deficiency and leads to uncontrolled immune activation. p.Tyr82Cys and p.Ile97Met TIM-3 pathogenic variants induce protein misfolding, abrogate expression of the receptor, and lead to the loss of the TIM-3 immune checkpoint and its multiple regulatory functions, promoting disease. TIM-3-mutant SPTCL should therefore be viewed as an inflammatory condition. Initial and possibly long-term control of the disease could be attained with immunosuppression and more novel agents targeting IL-1 and possibly IFN-γ that are both safe and effective in treating HLH–SPTCL.

Online content

Any methods, additional references, Nature Research reporting summaries, source data, statements of data availability and associated accession codes are available at https://doi.org/10.1038/s41588-018-0251-4.

Received: 5 March 2018; Accepted: 5 September 2018;
Published online: 29 October 2018

References

1. Willemze, R. et al. Subcutaneous panniculitis-like T-cell lymphoma: definition, classification, and prognostic factors: an EORTC Cutaneous Lymphoma Group Study of 83 cases. *Blood* **111**, 838–845 (2008).
2. Swerdlow, S. H. et al. The 2016 revision of the World Health Organization classification of lymphoid neoplasms. *Blood* **127**, 2375–2390 (2016).
3. Gonzalez, C. L., Medeiros, L. J., Braziel, R. M. & Jaffe, E. S. T-cell lymphoma involving subcutaneous tissue. A clinicopathologic entity commonly associated with hemophagocytic syndrome. *Am. J. Surg. Pathol.* **15**, 17–27 (1991).
4. Huppmann, A. R., Xi, L., Raffeld, M., Pittaluga, S. & Jaffe, E. S. Subcutaneous panniculitis-like T-cell lymphoma in the pediatric age group: a lymphoma of low malignant potential. *Pediatr. Blood Cancer* **60**, 1165–1170 (2013).
5. Willemze, R. Cutaneous lymphomas with a panniculitic presentation. *Semin. Diagn. Pathol.* **34**, 36–43 (2017).
6. Pincus, L. B. et al. Subcutaneous panniculitis-like T-cell lymphoma with overlapping clinicopathologic features of lupus erythematosus: coexistence of 2 entities? *Am. J. Dermatopathol.* **31**, 520–526 (2009).
7. Oschlies, I. et al. Subcutaneous panniculitis-like T-cell lymphoma in children: a detailed clinicopathological description of 11 multifocal cases with a high frequency of haemophagocytic syndrome. *Br. J. Dermatol.* **172**, 793–797 (2015).
8. Michonneau, D. et al. Subcutaneous panniculitis-like T-cell lymphoma: immunosuppressive drugs induce better response than polychemotherapy. *Acta Dermato-Venereol.* **97**, 358–364 (2017).
9. Gau, J. P. et al. Subcutaneous panniculitis-like T cell lymphoma: familial aggregation while different response to chemotherapy. *Int. J. Hematol.* **89**, 63–65 (2009).
10. Berg, K. D. et al. Transmission of a T-cell lymphoma by allogeneic bone marrow transplantation. *N. Engl. J. Med.* **345**, 1458–1463 (2001).
11. Monney, L. et al. Th1-specific cell surface protein Tim-3 regulates macrophage activation and severity of an autoimmune disease. *Nature* **415**, 536–541 (2002).
12. Sabatos, C. A. et al. Interaction of Tim-3 and Tim-3 ligand regulates T helper type 1 responses and induction of peripheral tolerance. *Nat. Immunol.* **4**, 1102–1110 (2003).
13. Sanchez-Fueyo, A. et al. Tim-3 inhibits T helper type 1-mediated auto- and alloimmune responses and promotes immunological tolerance. *Nat. Immunol.* **4**, 1093–1101 (2003).
14. Cao, E. et al. T cell immunoglobulin mucin-3 crystal structure reveals a galectin-9-independent ligand-binding surface. *Immunity* **26**, 311–321 (2007).
15. Hudjashov, G. et al. Investigating the origins of eastern Polynesians using genome-wide data from the Leeward Society Isles. *Sci. Rep.* **8**, 1823 (2018).
16. Anderson, A. C., Joller, N. & Kuchroo, V. K. Lag-3, Tim-3, and TIGIT: co-inhibitory receptors with specialized functions in immune regulation. *Immunity* **44**, 989–1004 (2016).
17. Das, M., Zhu, C. & Kuchroo, V. K. Tim-3 and its role in regulating anti-tumor immunity. *Immunol. Rev.* **276**, 97–111 (2017).
18. Kayser, M. et al. Genome-wide analysis indicates more Asian than Melanesian ancestry of Polynesians. *Am. J. Hum. Genet.* **82**, 194–198 (2008).
19. Schymkowitz, J. et al. The FoldX web server: an online force field. *Nucleic Acids Res.* **33**, W382–W388 (2005).
20. Pachlopnik Schmid, J. et al. Inherited defects in lymphocyte cytotoxic activity. *Immunol. Rev.* **235**, 10–23 (2010).
21. Takada, H. et al. Increased serum levels of interferon-γ-inducible protein 10 and monokine induced by gamma interferon in patients with haemophagocytic lymphohistiocytosis. *Clin. Exp. Immunol.* **133**, 448–453 (2003).
22. Wang, W. et al. Negative regulation of Nod-like receptor protein 3 inflammasome activation by T cell Ig mucin-3 protects against peritonitis. *Immunology* **153**, 71–83 (2018).
23. Sepulveda, F. E. & de Saint Basile, G. Hemophagocytic syndrome: primary forms and predisposing conditions. *Curr. Opin. Immunol.* **49**, 20–26 (2017).
24. Gautron, A.-S., Dominguez-Villar, M., de Marcken, M. & Hafler, D. A. Enhanced suppressor function of TIM-3$^+$FoxP3$^+$ regulatory T cells. *Eur. J. Immunol.* **44**, 2703–2711 (2014).
25. Greil, R., Hutterer, E., Hartmann, T. N. & Pleyer, L. Reactivation of dormant anti-tumor immunity—a clinical perspective of therapeutic immune checkpoint modulation. *Cell Commun. Signal.* **15**, 5 (2017).

Acknowledgements

This work was funded in part by the Foundation of Stars. N.J. is a member of the Penny Cole Laboratory and the recipient of a Chercheur Boursier, Chaire de Recherche Award from the Fonds de la Recherche du Québec en Santé. D.-A.K.-Q. is a Herman Clinical Fellow. We thank N. Brousse and the Groupe Français d'Etude des Lymphomes Cutanés for their valuable contributions. We also thank S. Lade from the Peter MacCallum

Cancer Centre and the Victorian Comprehensive Cancer Centre, Melbourne; P. McKelvie from the Department of Pathology at St. Vincent's Hospital Melbourne; D. MacGregor from the Department of Pathology at the Royal Children's Hospital (RCH) Melbourne; L. Dalla-Pozza from the Cancer Center for Children at The Children's Hospital at Westmead, Sydney; C. Picard from the Study Center of Immunodeficiencies (CEDI) at Hôpital-Necker Enfants Malades, Paris; and G. Ménasché from INSERM U1163 at Institut Imagine, Paris. The Children's Cancer Centre Tissue Bank at RCH Melbourne runs thanks to the generous support of Cancer in Kids @ RCH, Leukaemia Auxiliary at RCH, the Murdoch Children's Research Institute, and the RCH Foundation. The Tumour Bank at the Children's Hospital at Westmead is generously supported by the Kids Cancer Project. W.D.F. is funded by the Canadian Institute for Health Research (FDN-148390). The G.d.S.B. lab (INSERM 1163 at Institut Imagine) is Equipe labélisée Fondation pour la Recherche Médicale (FRM: DEQ20150734354) and is supported by l'Agence Nationale de la Recherche (ANR-12-BSV1-0020-01 and the Investissements d'Avenir program) and by the Fondation Imagine. A.F. is supported by Collège de France. T.G. and J.P. are recipients of Canadian Institutes of Health Research and Fonds de Recherche du Québec postdoctoral fellowships, respectively. A.B. is a recipient of a Fonds de Recherche du Québec doctoral studentship. E.T.V. was granted funding by Fundação de Amparo a Pesquisa do Estado de São Paulo (FAPESP, grant no. 2015/20142-0/Brazil), as part of a research fellowship abroad program to participate in this project. We thank M. Fu and S.-B. Feng of the Molecular Imaging facility at the Research Institute of the McGill University Health Centre for their assistance with the confocal microscope.

Author contributions

T.G., D.-A.K.-Q., J.P., E.T.V., A.G., S.K., F.S., L.G.M., N.H., M.T., A.B., S.D., D.D., D.S., and F.G. performed experiments and analyzed data. H.N., J.M., W.D.F., S.G., and R.D. analyzed data. D.Moshous, J.C., S.A., C.B.-F., P.N., B.B.-M., D.Mitchell, C.T., M.Battistella, V.-H.N., R.C., J.-S.D., C.M., H.M.P., M.Besnard, S.B., P.G.E., S.F., and A.F. contributed materials and analyzed data. F.E.S., B.N., D.Michonneau, G.d.S.B., and N.J. conceived and designed the experiments and analyzed data. All authors contributed to the written manuscript.

Competing interests

The authors declare no competing interests.

Additional information

Supplementary information is available for this paper at https://doi.org/10.1038/s41588-018-0251-4.

Reprints and permissions information is available at www.nature.com/reprints.

Correspondence and requests for materials should be addressed to G.B. or N.J.

Publisher's note: Springer Nature remains neutral with regard to jurisdictional claims in published maps and institutional affiliations.

Methods

Patient samples and clinical information. This study was approved by the institutional review boards of the respective institutions from which the samples were collected. Patients had an institutional diagnosis of SPTCL. Tumor samples and constitutive DNA, clinical data, ethnic background, and outcome were collected from all probands and TIM-3-mutant family members whenever possible (Table 1 and Supplementary Table 1). A total of 27 patients with institutional diagnosis of SPTCL were recruited, including three families, two from East Asia with two affected siblings each (P1 and P2; P10 and P11) and another from French Polynesia with one affected child (P4). Unaffected family members were also recruited when available. Matched blood samples were available for 13 cases (11 with TIM-3 alteration). The tumor samples are composed of 22 formalin-fixed paraffin-embedded (FFPE) samples and 4 fresh-frozen tissues. Patients' ages ranged from 1 to 90 years (median 19 years), and their ethnic backgrounds included European ($n=12$), Polynesian ($n=8$), East Asian ($n=4$), African ($n=2$), and South American ($n=1$) ancestry (Supplementary Table 1). Detailed case reports of TIM-3-mutant SPTCL patients are provided in the Supplementary Note.

DNA isolation. Genomic DNA was extracted from peripheral blood and frozen tumor tissue using the QIAamp DNA Blood Mini Kit (Qiagen) and the QIAamp DNA Micro Kit (Qiagen), respectively. DNA from FFPE samples was isolated with the QIAamp DNA FFPE Tissue Kit (Qiagen).

WES. WES was performed on constitutive DNA and tumor material whenever possible (Supplementary Table 1). Exomes were captured using either the Agilent SureSelect V5 or V6 kits according to the manufacturer's instructions. The enriched libraries were sequenced on the Illumina HiSeq 2500 and 4000 systems with 125-base pair (bp) and 100-bp paired-end reads, respectively. WES data were analyzed for variants using the GenPipes pipeline. This pipeline follows the stepwise procedures of the Broad Institute Genome Analysis Toolkit (GATK) best practices. Raw reads derived from the sequencing instrument are quality-trimmed and adapter-clipped using Trimmomatic[26] to obtain a high-quality set of reads for sequence alignment (Sequence Alignment Map (SAM)/Binary Alignment Map (BAM)) file generation. The trimmed reads are aligned to a reference genome (build 37) using a fast, memory-efficient Burrows-Wheeler transform aligner BWA-mem[27]. Mapped reads are further refined using GATK[28] and Picard program suites (http://broadinstitute.github.io/picard) to improve mapping near insertions and deletions (indels; GATK indel realigner), remove duplicate reads with the same paired start site (Picard mark duplicates), and improve quality scores (GATK base recalibration). Variants are called using the GATK haplotype caller in gvcf mode to allow efficient downstream merging of multiple samples into one variant file to streamline downstream variant processing procedures, which include normalization and decomposition of multinucleotide polymorphisms[29], functional annotation with SNPeff[30], and variant annotations using the Gemini[31] framework, which provides quality metric and extensive metadata to help further prioritize variants. Annotated variants were filtered against the common germline polymorphisms present in dbSNP135, the 1000 Genomes Project[32], and gnomAD. Somatic mutations were called by comparing variants from the matched tumor–normal pairs. A summary of WES metrics is provided in Supplementary Table 2.

Sanger sequencing. Primers flanking exon 2 of the *HAVCR2* gene were used to screen and validate the mutations identified by WES on constitutive DNA and tumor material for all the cases available in our SPTCL cohort. The purified PCR products were then bidirectionally sequenced on an ABI 3730XL DNA Analyzer (Applied Biosystems). Primers and PCR conditions are available upon request.

Haplotype analysis. Haplotype analysis was performed as previously described[33]. PCR primers were designed to amplify short tandem repeat markers for six markers spanning a 3.1-megabase region on chromosome 5q that includes *HAVCR2* (TIM-3). PCR products were radiolabeled using T4 polynucleotide kinase (Thermo Fisher Scientific) to add the radiolabel ^{33}P (γ-^{33}P-ATP from PerkinElmer) to the 5′ end of the PCR primers prior to amplification. Amplified products were separated by electrophoresis on a 5% or 6% denaturing acrylamide-urea gel and then autoradiographed. Primer sequences and amplification conditions are available on request.

Protein-folding assay. Wild-type, Tyr82Cys, and Ile97Met IgV domains of human TIM-3 (residues 22–130) were cloned into the bacterial expression vector pET-SUMO using NdeI and XhoI cut sites (to avoid the SUMO fusion). Each protein was expressed in *Escherichia coli* BL21 cells grown in LB media supplemented with 50 μg ml^{-1} kanamycin to form insoluble inclusion bodies. The inclusion bodies were purified using the method previously described for the mouse homolog of the TIM-3 IgV domain[14]. Protein refolding was accomplished by diluting the inclusion bodies solubilized in 10 mM sodium acetate, 6 M guanidinium hydrochloride, 5 mM EDTA, and 1 mM dithiothreitol, pH 4.6, 100-fold into a buffer containing 200 mM Tris-HCl, 0.4 M arginine-HCl, 2 mM EDTA, 5 mM cysteamine, and 0.5 mM cystamine, pH 9.0. Refolded proteins were concentrated to 0.50–0.75 mg ml^{-1} using Amicon Ultra-15 centrifugal filter units with a 3 kDa molecular weight cut-off and then dialyzed against a buffer containing 10 mM Tris-HCl and 20 mM NaCl, pH 8.0. Precipitated protein was removed by centrifugation before final analysis of a 1 ml protein sample on a Superdex G-75 24 ml size-exclusion column. Eluted fractions (1 ml) were analyzed using 15% SDS–PAGE gels, and properly folded protein monomers were detected by their elution at 16 ml.

Construction of expression vector and lentiviral infection. The FLAG-tagged coding sequence of human *HAVCR2* or TIM-3 (NM_032782) was purchased as a synthetic gBlock from Integrated DNA Technologies and cloned into the inducible pLVX-TetOne-Puro vector using In-Fusion Cloning (Clontech). TIM-3 mutants p.Tyr82Cys and p.Ile97Met were generated by PCR-based site-directed mutagenesis of the wild-type TIM-3 construct using the In-Fusion Cloning Kit from Clontech. The constructs were transformed into stellar competent cells, amplified, and confirmed using restriction enzyme digestion (BamHI and EcoRI) as well as conventional Sanger sequencing with the primers that were originally used to amplify the TIM-3 complementary DNA. Lentiviral supernatants were produced by transfecting 293LTV packaging cells with Lenti-X Packaging Single Shots (vesicular stomatitis virus-glycoprotein) and pLVX-TetOne-Puro vectors (Clontech) containing wild-type and mutant TIM-3 sequences. Lentiviral supernatant was collected at 18, 26, and 42 h after transfection and filtered through 0.45 μm filters. Lentiviral particles were concentrated by ultracentrifugation at 41,200*g* for 2 h at 4 °C, resuspended in basal medium, and stored at −80 °C. HEK293 cells were transduced with lentiviral particles, and stable clones were selected with 10 μg ml^{-1} puromycin 48 h post-infection.

Cell culture. Stable HEK293 transduced cell lines (wild-type TIM-3, p.Tyr82Cys TIM-3, and p.Ile97Met TIM-3) were cultured in the presence of puromycin selection and DMEM complete medium (4.5 g l^{-1} glucose, 0.11 g l^{-1} sodium pyruvate, 0.58 g l^{-1} L-glutamine, and 10% FBS). Parental HEK293 cells were used as a control. All cell lines were maintained at 37 °C with 95% air and 5% CO_2. At 90% confluency, the cells were counted and re-plated in complete medium supplemented with puromycin. The expression of TIM-3 was induced by adding 1 μg ml^{-1} doxycycline to the complete medium for 24 h.

Immunoblotting. Cells were washed with PBS and collected in lysis buffer (10 mM Tris-HCl (pH 7.5), 1% Triton X-100, 0.5% IgePal, 150 mM NaCl, and 1 mM EDTA) containing protease and phosphatase inhibitors. Lysates were quantified by the Bradford method using BSA as a standard. Proteins were separated by SDS–PAGE, electrotransferred to polyvinylidene difluoride membranes, and blocked for 1 h at room temperature with 5% nonfat dry milk in Tris-buffered saline (150 mM NaCl, 20 mM Tris-HCl, pH 7.5) containing 0.3% Tween 20 (Amresco: 0777-1L) (TBST). Membranes were washed and incubated overnight at 4 °C with anti-TIM-3 (1:1,000; CST 45208) and anti-FLAG (1:1,000; CST 2368) primary antibodies. Anti-β-actin (1:10,000; CST 4970) was used as a loading control. Membranes were washed with TBST and incubated with horseradish peroxidase (HRP)-conjugated anti–rabbit IgG secondary antibody (1:5,000, NA934V) for 1 h at room temperature. Immunoreactive material was revealed using Amersham ECL prime detection (Amersham Biosciences) and the ChemiDoc MP imaging system (BioRad).

Immunofluorescence. Cells were plated onto cover-slips and treated with 1 μg ml^{-1} doxycycline for 24 h. Medium was removed, and cells were fixed in 4% formaldehyde in PBS for 20 min. Cells were permeabilized with 0.2% Triton X-100 for 10 min and blocked for 6 h in a PBS solution containing 3% BSA and 3% normal goat serum or blocked immediately. Immunostaining was performed overnight at 4 °C with anti-TIM-3 (1:500, diluted in blocking solution), followed by Alexa Fluor 488 goat anti–rabbit IgG (H + L) secondary antibody (1:500, diluted in blocking solution). Cover-slips were mounted to microscope slides with ProLong Gold Antifade Mountant with 4,6-diamidino-2-phenylindole (DAPI) (Molecular Probes, Life Technologies, P36935). Images were finally taken using a Zeiss LSM780 laser scanning confocal microscope with a 63×/1.40 Oil Plan-Apochromat objective and analyzed with ZEN 2010 software (blue edition, Carl Zeiss Microscopy).

Dual immunofluorescence was performed on slides from SPTCL biopsies. Briefly, CD4 (Clone SP35, Roche) and FOXP3 (Clone 236A/E7, Abcam) diluted in the antibody diluent (No. 251-018, Roche) (CD4, prediluted; FOXP3, 1:50) were manually applied for 32 min at 37 °C. This was followed by application of the appropriate detection kit—OmniMap anti-Rb HRP (No. 760-4311, Roche) or OmniMap anti-Ms HRP (No. 760-4310, Roche) for 8 min—followed by the Discovery Rhodamine Kit (No. 760-233, Roche) and the Discovery FITC Kit (No. 760-232, Roche) for 12 min. A negative control was obtained through omitting primary antibodies. The detection for each marker was completed before application of the next antibody. Slides were removed from the autostainer, washed in warm soapy water to remove the oil cover-slip, rinsed with PBS, counterstained with DAPI for 5 min, then mounted with a mounting medium (Immu-Mount, Thermo Fisher Scientific). Images were acquired with a confocal microscope, and cells positive for FOXP3 and CD4 staining were counted using Fiji software (1.50e). Images were assembled using Photoshop.

Flow cytometry. After 24 h of induction with 1 µg ml^{-1} doxycycline, HEK293T cells were collected and resuspended in a solution of binding buffer. Cells were then incubated for 1 h at room temperature in the dark with either the antigen-presenting cell rat anti-human Tim-3 antibody or the rat IgG2A isotype control antibody. The cells were washed three times and resuspended in PBS. Fluorescence was then visualized by flow cytometry using a FACSCalibur (FL4 channel) and the CellQuest Pro software (v5.2) (BD Biosciences).

Expression of TIM-3 on monocytes (CD14$^+$) and phytohemagglutinin-induced T lymphoblasts (CD4$^+$CD8$^+$) from patients and healthy individuals was measured using flow cytometry. Murine monoclonal antibodies to CD4 and CD8, isotype control antibody, and Fc blocking reagent were from Miltenyi Biotec. Anti-CD14 was from BD Biosciences.

Purification of blood monocytes and differentiation of macrophages. Monocytes were purified from peripheral blood mononuclear cells of healthy blood donors or patients using positive selection (CD14 beads, BD Biosciences). To obtain in vitro-derived monocyte-derived macrophages, monocytes were cultured for 5 d in RPMI 1640-GlutaMAX supplemented with 10% FCS medium of 50 ng ml^{-1} macrophage colony-stimulating factor (M-CSF) (Sigma) and 1% penicillin–streptomycin.

Monocyte-derived macrophage activation and quantification of cytokine production. To measure cytokine production upon TLR stimulation, 10^6 monocyte-derived macrophages were activated with different doses of LPS (InvivoGen) for 16 h in RPMI 1640-GlutaMAX supplemented with 10% FCS medium of 50 ng ml^{-1} M-CSF and 1% penicillin–streptomycin. To measure cytokine production upon inflammasome activation, monocyte-derived macrophages were primed for 16 h with 5 ng ml^{-1} LPS followed by 1 h stimulation with 1 µM nigericin (a NLRP3 agonist) (Sigma). Secretion of inflammatory cytokines was assessed by a BD Cytometric Bead Array (CBA) Human Inflammatory Cytokines Kit, according to the manufacturer's instructions (BD Biosciences).

Cytokine quantification. Phytohemagglutinin-induced T lymphoblasts were cultured for 15 d in presence of IL-2[34], and supernatants were collected after anti-CD3 activation for 1 h. Production of inflammatory cytokines in lymphoblasts' supernatants and in the plasma of healthy controls and patients was assessed by a BD Cytometric Bead Array (CBA) Human Inflammatory Cytokines Kit, according to the manufacturer's instructions (BD Biosciences). Soluble CD25 concentration was determined using a Quantikine ELISA kit (R&D Systems). CXCL10 concentration was measured using an ELISA Max Deluxe kit (BioLegend). IL-18 concentration was quantified using an IL-18 ELISA kit from Invitrogen (Thermo Fisher Scientific).

Degranulation assay. A degranulation assay was performed on T lymphoblasts from healthy controls and patients as previously described[34]. Monoclonal murine anti-CD3 antibody was purchased from Miltenyi Biotec.

Statistics. Statistical analyses were performed using GraphPad Prism software and Microsoft Excel. All the statistical tests used were described in the relevant sections of the manuscript. P-values < 0.05 were considered statistically significant.

Reporting Summary. Further information on research design is available in the Nature Research Reporting Summary linked to this article.

Data availability

Raw exome sequence data have been deposited at the European Genome-phenome Archive (EGA), which is hosted by the European Bioinformatics Institute (EMBL-EBI) and the Centre for Genomic Regulation (CRG), under accession number EGAS00001002765.

References

26. Bolger, A. M., Lohse, M. & Usadel, B. Trimmomatic: a flexible trimmer for Illumina sequence data. *Bioinformatics* **30**, 2114–2120 (2014).
27. Li, H. & Durbin, R. Fast and accurate long-read alignment with Burrows-Wheeler transform. *Bioinformatics* **26**, 589–595 (2010).
28. McKenna, A. et al. The Genome Analysis Toolkit: a MapReduce framework for analyzing next-generation DNA sequencing data. *Genome Res.* **20**, 1297–1303 (2010).
29. Tan, A., Abecasis, G. R. & Kang, H. M. Unified representation of genetic variants. *Bioinformatics* **31**, 2202–2204 (2015).
30. Cingolani, P. et al. A program for annotating and predicting the effects of single nucleotide polymorphisms, SnpEff: SNPs in the genome of *Drosophila melanogaster* strain *w*^{1118}; *iso*-2; *iso*-3. *Fly* **6**, 80–92 (2012).
31. Paila, U., Chapman, B. A., Kirchner, R. & Quinlan, A. R. GEMINI: integrative exploration of genetic variation and genome annotations. *PLoS Comput. Biol.* **9**, e1003153 (2013).
32. 1000 Genomes Project Consortium. A map of human genome variation from population-scale sequencing. *Nature* **467**, 1061–1073 (2010).
33. Hamel, N. et al. On the origin and diffusion of *BRCA1* c.5266dupC (5382insC) in European populations. *Eur. J. Hum. Genet.* **19**, 300–306 (2011).
34. Cote, M. et al. Munc18-2 deficiency causes familial hemophagocytic lymphohistiocytosis type 5 and impairs cytotoxic granule exocytosis in patient NK cells. *J. Clin. Investig.* **119**, 3765–3773 (2009).

nature research

Corresponding author(s): Nada Jabado , Genevieve de Saint Basile

Reporting Summary

Nature Research wishes to improve the reproducibility of the work that we publish. This form provides structure for consistency and transparency in reporting. For further information on Nature Research policies, see Authors & Referees and the Editorial Policy Checklist.

Statistical parameters

When statistical analyses are reported, confirm that the following items are present in the relevant location (e.g. figure legend, table legend, main text, or Methods section).

n/a	Confirmed	
☐	☒	The exact sample size (*n*) for each experimental group/condition, given as a discrete number and unit of measurement
☐	☒	An indication of whether measurements were taken from distinct samples or whether the same sample was measured repeatedly
☐	☒	The statistical test(s) used AND whether they are one- or two-sided *Only common tests should be described solely by name; describe more complex techniques in the Methods section.*
☒	☐	A description of all covariates tested
☒	☐	A description of any assumptions or corrections, such as tests of normality and adjustment for multiple comparisons
☐	☒	A full description of the statistics including central tendency (e.g. means) or other basic estimates (e.g. regression coefficient) AND variation (e.g. standard deviation) or associated estimates of uncertainty (e.g. confidence intervals)
☒	☐	For null hypothesis testing, the test statistic (e.g. *F*, *t*, *r*) with confidence intervals, effect sizes, degrees of freedom and *P* value noted *Give P values as exact values whenever suitable.*
☒	☐	For Bayesian analysis, information on the choice of priors and Markov chain Monte Carlo settings
☒	☐	For hierarchical and complex designs, identification of the appropriate level for tests and full reporting of outcomes
☒	☐	Estimates of effect sizes (e.g. Cohen's *d*, Pearson's *r*), indicating how they were calculated
☐	☒	Clearly defined error bars *State explicitly what error bars represent (e.g. SD, SE, CI)*

Our web collection on statistics for biologists may be useful.

Software and code

Policy information about availability of computer code

Data collection	No software was used for data collection.
Data analysis	Exome data was analyzed using DNA-Seq pipeline (Genpipes v 3.1.0, source codes available at https://bitbucket.org/mugqic/genpipes/src). The pipeline uses following codes/softwares, namely Trimmomatic (v 0.35), BWA-mem (v 0.7.15), GATK (v 3.8), Picard (v 2.9.0), SNPeff (v 4.3) and Gemini (v 0.20.1). Confocal microscopy was analyzed in ZEN 2010 (blue edition, Carl Zeiss Microscopy GmbH, 2011). FOXP3 and CD4 positive cells were counted with Fiji software (1.50e). IHC and confocal images were assembled using photoshop CS6. FACS data was analyzed using CellQuest Pro (v 5.2) and Flow Jo (10.4) softwares .

For manuscripts utilizing custom algorithms or software that are central to the research but not yet described in published literature, software must be made available to editors/reviewers upon request. We strongly encourage code deposition in a community repository (e.g. GitHub). See the Nature Research guidelines for submitting code & software for further information.

Data

Policy information about availability of data

All manuscripts must include a data availability statement. This statement should provide the following information, where applicable:

- Accession codes, unique identifiers, or web links for publicly available datasets
- A list of figures that have associated raw data
- A description of any restrictions on data availability

Sequence data has been deposited at the European Genome-phenome Archive (EGA), which is hosted by the EBI and the CRG, under accession number EGAS00001002765.

Field-specific reporting

Please select the best fit for your research. If you are not sure, read the appropriate sections before making your selection.

☒ Life sciences ☐ Behavioural & social sciences ☐ Ecological, evolutionary & environmental sciences

For a reference copy of the document with all sections, see nature.com/authors/policies/ReportingSummary-flat.pdf

Life sciences study design

All studies must disclose on these points even when the disclosure is negative.

Sample size	No statistical method was used to predetermine sample size. Sub-cutaneous panniculitis-like T-cell lymphomas (STPCL) is a rare disorder and we collected as many patients as possible, both locally and internationally through our collaborators.
Data exclusions	No data were excluded.
Replication	Experiments were replicated and confirmed.
Randomization	Randomization was not relevant to this study because patients were accrued from retrospective cohorts based on their diagnosis of SPTCL.
Blinding	Blinding was not relevant to this study since all patients were clinically diagnosed as SPTCL and their TIM3 mutation status was identified using WES and/or Sanger.

Reporting for specific materials, systems and methods

Materials & experimental systems

n/a	Involved in the study
☐	☒ Unique biological materials
☐	☒ Antibodies
☐	☒ Eukaryotic cell lines
☒	☐ Palaeontology
☒	☐ Animals and other organisms
☐	☒ Human research participants

Methods

n/a	Involved in the study
☒	☐ ChIP-seq
☐	☒ Flow cytometry
☒	☐ MRI-based neuroimaging

Unique biological materials

Policy information about availability of materials

Obtaining unique materials	All unique materials used are available upon request following MTA.

Antibodies

Antibodies used	anti-TIM-3 (CST 45208), anti-FLAG (CST 2368), anti-β-Actin (CST 4970), HRP-conjugated anti-rabbit IgG secondary antibody (NA934V, GE Healthcare Life Sciences), Alexa Fluor 488 goat anti-rabbit IgG (A-11008, ThermoFisher Scientific), CD8 FITC mouse anti-human IgG1, k (345772, BD Biosciences), CD4 PE mouse anti-human IgG1, k (345768, BD Biosciences), CD8-APC-Vio770 ™ recombinant anti-human IgG1 (130-110-680, Miltenyi Biotec), CD4- VioBlue mouse anti-human IgG2a (130-¬113-¬219, Miltenyi

Biotec), Pacific Blue™ Mouse Anti-Human CD14 IgG2a, κ (558121, BD Biosciences), Human TIM-3 APC-conjugated Antibody Rat IgG2A (FAB2365A R&D Systems), CD4 (Clone SP35, Roche), FOXP3 (Clone 236A/E7, abcam)

Validation

anti-TIM-3 (CST 45208),
Species: Human
Application: WB, IP, IHC, F
https://www.cellsignal.com/products/primary-antibodies/tim-3-d5d5r-xp-rabbit-mab/45208

anti-FLAG (CST 2368),
Species: N/A
Application: WB, IP, F
https://www.cellsignal.com/products/primary-antibodies/dykddddk-tag-antibody-binds-to-same-epitope-as-sigma-s-anti-flag-m2-antibody/2368

anti-β-Actin (CST 4970),
Species: Human, Mouse, Rat, Monkey, Bovine, Pig
Application: WB, IHC, IF, F
https://www.cellsignal.com/products/primary-antibodies/b-actin-13e5-rabbit-mab/4970

HRP-conjugated anti-rabbit IgG secondary antibody (NA934V, GE Healthcare Life Sciences),
Species: Rabbit, Human
Application: WB
https://www.citeab.com/antibodies/3288288-na934-100ul-amersham-ecl-rabbit-igg-hrp-linked-whol

Alexa Fluor 488 goat anti-rabbit IgG (A-11008, ThermoFisher Scientific),
Species: Rabbit
Application: ICC, IF, F
https://www.thermofisher.com/antibody/product/Goat-anti-Rabbit-IgG-H-L-Cross-Adsorbed-Secondary-Antibody-Polyclonal/A-11008

CD8 FITC mouse anti-human IgG1, k (345772, BD Biosciences)
Species: Human
Application: Flow cytometry
https://www.bdbiosciences.com/eu/reagents/clinical/reagents/single-antibodies/cd8-fitc-sk1/p/345772

CD4 PE mouse anti-human IgG1, k (345768, BD Biosciences)
Species: Human
Application: Flow cytometry
https://www.bdbiosciences.com/eu/reagents/clinical/reagents/single-antibodies/cd4-fitc-sk3-also-known-as-leu3a/p/345768

CD8-APC-Vio770 ™ recombinant anti-human IgG1 (130-110-680, Miltenyi Biotec)
Species: Human
Application: Flow cytometry
http://www.miltenyibiotec.com/~/media/Images/DatasheetGeneration/Datasheets/39400/39400/DS_CD8_PE_Vio770__human_REA734.ashx?force=1

CD4- VioBlue mouse anti-human IgG2a (130-¬113-¬219, Miltenyi Biotec)
Species: Human
Application: Flow cytometry
http://www.miltenyibiotec.com/~/media/Images/DatasheetGeneration/Datasheets/42700/42720/DS_CD4_VioBlue__human_VIT4.ashx?force=1

Pacific Blue™ Mouse Anti-Human CD14 IgG2a, κ (558121, BD Biosciences)
Species: Human
Application: Flow cytometry
http://www.bdbiosciences.com/eu/applications/research/stem-cell-research/hematopoietic-stem-cell-markers/human/negative-markers/pacific-blue-mouse-anti-human-cd14-m5e2/p/558121

Human TIM-3 APC-conjugated Antibody Rat IgG2A (FAB2365A R&D Systems)
Species: Human
Application: Flow cytometry
https://www.rndsystems.com/products/human-tim-3-apc-conjugated-antibody-344823_fab2365a

CD4 (Clone SP35, Roche)
Species: Rabbit
Application: Immunoflourence
http://ventana.com/product/31?type=26

FOXP3 (Clone 236A/E7, abcam)
Species: Mouse
Application: Immunoflourence
https://www.abcam.com/foxp3-antibody-236ae7-ab20034.html

Eukaryotic cell lines

Policy information about cell lines

Cell line source(s)	HEK293 cells were purchased from ATCC.
Authentication	We used the GenePrint 10 STR kit from Promega to authenticate the HEK293 cell line.
Mycoplasma contamination	HEK293 cell line was regularly tested for mycoplasma and found to be negative.
Commonly misidentified lines (See ICLAC register)	HEK293 cells are easy to culture and they exhibit high transfection efficiency.

Human research participants

Policy information about studies involving human research participants

Population characteristics	Patient's age ranged from 1 to 90 years (median 19 years) and their ethnic backgrounds include Caucasian (n=12), Polynesian (n=8), East Asian (n=4), African (n=2) and South American (n=1). 16 of 27 SPTCL patients are TIM3 mutants and their median age is younger than those that are TIM3-WT (n=11).
Recruitment	Sub-cutaneous panniculitis-like T-cell lymphomas (STPCL) is a rare disorder and we collected as many patients as possible, both locally and internationally through our collaborators.

Flow Cytometry

Plots

Confirm that:

☒ The axis labels state the marker and fluorochrome used (e.g. CD4-FITC).

☒ The axis scales are clearly visible. Include numbers along axes only for bottom left plot of group (a 'group' is an analysis of identical markers).

☒ All plots are contour plots with outliers or pseudocolor plots.

☒ A numerical value for number of cells or percentage (with statistics) is provided.

Methodology

Sample preparation	After 24 hrs of induction with 1 µg/ml doxycycline, HEK293 cells were harvested and resuspended in a solution of binding buffer. Cells were then incubated for 1 hr at room temperature in the dark with either the APC rat anti-human Tim-3 antibody or the rat IgG2A isotype control antibody. The cells were washed three times and resuspended in PBS. After Ficoll purification, PBL were washed twice in PBS + 2mM EDTA + 0,5 mg/mL BSA. Cells were incubated for 20 minutes at 4° C in darkness in the presence of relevant antibodies. After the incubation, cells were washed and resuspended in the same buffer.
Instrument	BD FACSCalibur (FL4 channel) Ref 342975. / Gallios flow cytometer, BeckmanCoulter
Software	CellQuest Pro software / FlowJo
Cell population abundance	No sorting was performed.
Gating strategy	Cells were gated based on FCS/SSC followed by selection of CD4, CD8 or CD14 positive cells.

☐ Tick this box to confirm that a figure exemplifying the gating strategy is provided in the Supplementary Information.